Programming colloidal bonding using DNA strand-displacement circuitry

Xiang Zhou[a,1], Dongbao Yao[a,1,2], Wenqiang Hua[b], Ningdong Huang[c], Xiaowei Chen[c], Liangbin Li[c,2], Miao He[a], Yunhan Zhang[a], Yijun Guo[a], Shiyan Xiao[a,2], Fenggang Bian[b,2], and Haojun Liang[a,2]

[a]CAS Key Laboratory of Soft Matter Chemistry, Hefei National Laboratory for Physical Sciences at the Microscale, Collaborative Innovation Center of Chemistry for Energy Materials, University of Science and Technology of China, 230026 Hefei, Anhui, P. R. China; [b]Shanghai Synchrotron Radiation Facility, Zhangjiang Laboratory, Shanghai Advanced Research Institute, Chinese Academy of Sciences, 201204 Shanghai, P. R. China; and [c]National Synchrotron Radiation Lab, CAS Key Laboratory of Soft Matter Chemistry, University of Science and Technology of China, 230026 Hefei, Anhui, P. R. China

Edited by Chad A. Mirkin, Northwestern University, Evanston, IL, and approved February 10, 2020 (received for review October 14, 2019)

As a strategy for regulating entropy, thermal annealing is a commonly adopted approach for controlling dynamic pathways in colloid assembly. By coupling DNA strand-displacement circuits with DNA-functionalized colloid assembly, we developed an enthalpy-mediated strategy for achieving the same goal while working at a constant temperature. Using this tractable approach allows colloidal bonding to be programmed for synchronization with colloid assembly, thereby realizing the optimal programmability of DNA-functionalized colloids. We applied this strategy to conditionally activate colloid assembly and dynamically switch colloid identities by reconfiguring DNA molecular architectures, thereby achieving orderly structural transformations; leveraging the advantage of room-temperature assembly, we used this method to prepare a lattice of temperature-sensitive proteins and gold nanoparticles. This approach bridges two subfields: dynamic DNA nanotechnology and DNA-functionalized colloid programming.

colloid assembly | programmable colloidal bonding | enthalpy-mediated strategy | DNA strand-displacement circuitry | structural transformation

Self-assembly is a thermodynamically driven nonequilibrium process, which is easily trapped at intermediate local free-energy minima, resulting in an unexpected malformed structure (1–3) rather than reaching a global free-energy minimum and producing ordered structures. Therefore, effective ways to evade each local free-energy minimum are highly desired. Consider that free energy is a thermodynamic state function that relies solely on the initial and final state and is independent of dynamic pathways. This advantage allows the rational design of arbitrary dynamic pathways toward a global free-energy minimum. In the free-energy change equation, $\Delta G = \Delta H - K_B T \Delta S$, a negative enthalpy generally contributes to aggregation, while entropy leads to dispersion. In terms of the mathematical definition of temperature, $T = (\partial U/\partial S)_{V,N}$, $1/T$ represents the driving force for guiding a system toward the maximum entropy corresponding to a free-energy minimum (4). In the case of an energy-invariant system, where the internal energy accounting for the total interactions between particles is immutable, enthalpy is difficult, if not impossible, to regulate. Then, the temperature capability of tuning entropy has become the exclusive option for controlling dynamic pathways, conventionally realized via a time-dependent temperature scheme called thermal annealing. Considering that attraction between particles drives a system to an enthalpy minimum, we are inspired to explore whether interactions between particles can be programmed in a time-dependent manner for controlling dynamic pathway to achieve a free-energy minimum in a temperature-invariant system. The purpose of this research is to explore and solve this interesting problem.

Consider that inorganic colloidal nanoparticles functionalized with a layer of DNA molecules, known as "programmable atom equivalents" (PAEs) (5–7), can be programmed via design of the base sequences of the DNA molecules. To date, PAEs have shown powerful programmability in building three-dimensional colloidal superlattices (8–11), realizing colloidal phase transitions (12), and regulating interactions between nanoparticles (13). Colloidal particles endowed with time-dependent interactions were also suggested as a promising way of constructing artificial systems having properties of living systems (14, 15). Here we create a system that allows PAE bonding to be programmed, whereby we can explore whether it is possible to realize an ordered structure corresponding to the free-energy minimum under time-dependent interaction control.

In the field of dynamic DNA nanotechnology, a reaction referred to as toehold-mediated strand-displacement reaction (TMSDR) (16) provides a powerful solution for programming DNA assembly (17–20). With the participation of this versatile reaction, we establish a time-dependent interaction system via cascading two subsystems (Fig. 1*A*): (i) a catassembly DNA-circuit subsystem (18, 21) that is catalytically driven by a *Catassembler* strand via TMSDRs to controllably release the *Trigger* strands; (ii) a PAEs-based subsystem that is initiated by the *Trigger* strands released from the catassembly DNA circuit to assemble PAEs into different structures.

Results and Discussion

Constructing Time-Dependent Interaction System. As shown in Fig. 1*A*, the catassembly DNA-circuit subsystem is composed of a

Significance

We developed an enthalpy-mediated strategy to control dynamic pathways in colloidal assembly by working at constant temperature, which provides a different option to circumvent metastability that normally causes disordered structures. Using this tractable approach allows colloidal bonding to be programmed for synchronization with colloid assembly, thereby realizing the optimal programmability of DNA-functionalized colloids. Moreover, the dynamic conversion of the colloidal identity can be easily achieved using this method, i.e., the conversion of colloid-A to colloid-B during colloidal assembly. This approach represents an important step for nanoscientists to manipulate colloidal bonds to create complex and functional nanoscale materials, just as chemists manipulate atomic bonds to synthesize complex and functional molecules.

Author contributions: X.Z., D.Y., and H.L. designed research; X.Z. and D.Y. performed research; X.Z., D.Y., M.H., Y.Z., Y.G., S.X., and H.L. analyzed data; X.Z., D.Y., and H.L. wrote the paper; W.H., N.H., X.C., L.L., and F.B. contributed to the SAXS measurements; and S.X. performed theoretical analyses.

The authors declare no competing interest.

This article is a PNAS Direct Submission.

[1]X.Z. and D.Y. contributed equally to this work.

[2]To whom correspondence may be addressed. Email: dbyao@ustc.edu.cn, lbli@ustc.edu.cn, xiaosy@ustc.edu.cn, bianfenggang@zjlab.org.cn, or hjliang@ustc.edu.cn.

This article contains supporting information online at https://www.pnas.org/lookup/suppl/doi:10.1073/pnas.1917941117/-/DCSupplemental.

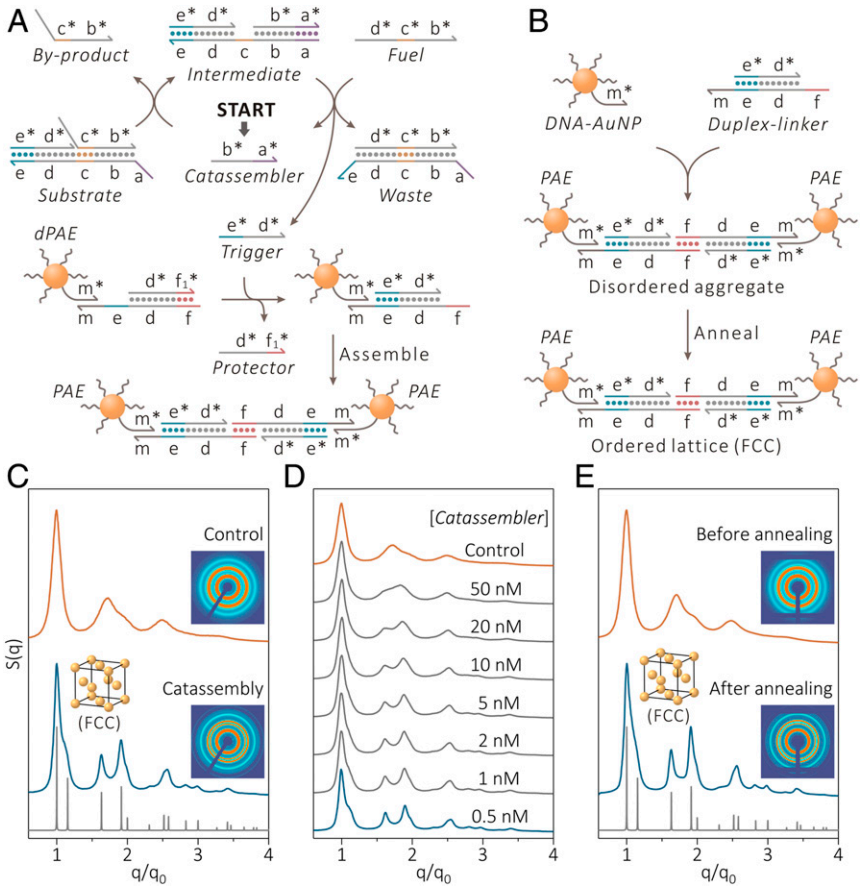

Fig. 1. PAE assembly in a unary system via a temperature-invariant time-dependent interaction scheme and an energy-invariant thermal annealing strategy. (*A*) Scheme of PAE assembly driven by a DNA strand-displacement circuit. (*B*) Scheme of PAE assembly with a thermal annealing strategy. (*C*) SAXS patterns for PAE aggregates formed by adding a full amount of *Trigger* (1.5 μM) with a 60:1 molar ratio of *Trigger*-to-*dPAE* (disordered aggregate shown in the "Control" curve) and 0.5-nM *Catassembler* (FCC lattice shown in the "Catassembly" curve) in a time-dependent interaction system. (*D*) SAXS data for PAE aggregates with the amount of *Catassembler* varied from 50 to 0.5 nM, indicating PAE aggregates changing from disordered to ordered structures. Here, [*dPAE*] = 25 nM, [*Duplex-linker′*] = 750 nM, [*Substrate*] = 1.5 μM, and [*Fuel*] = 3 μM. (*E*) SAXS data for PAE aggregates formed by adding a full amount of *Duplex-linker* into the energy-invariant system before (disordered aggregate shown in the "Before annealing" curve) and after thermal annealing (FCC lattice shown in the "After annealing" curve). Here, [*PAE*] = 25 nM, [*Duplex-linker*] = 750 nM. The gray lines at the *Bottom* of *C* and *E* represent theoretical SAXS patterns for a perfect FCC lattice.

dual hybridized DNA complex named *Substrate* (made of three single strands: *Bottom-substrate*, *By-product*, and *Trigger*; *SI Appendix*, Fig. S1) and a single-stranded *Fuel* strand; the PAEs-based subsystem is constructed with DNA-functionalized gold nanoparticles (DNA-AuNPs) and DNA complexes (*Duplex-linker* in *SI Appendix*, Fig. S5*A* and *Duplex-linker′* in *SI Appendix*, Fig. S5*B*). The deactivated PAE having protected sticky ends is defined as "*dPAE*" (Fig. 1*A* and *SI Appendix*, Fig. S5*B*) to distinguish it from the "*PAE*" having active sticky ends (Fig. 1*B* and *SI Appendix*, Fig. S5*A*). The brief reaction scheme for system operation is shown in Fig. 1*A* (detailed reaction steps are given in *SI Appendix*, sections S2.1 and S2.2). In the catassembly DNA-circuit subsystem, upon addition of *Catassembler*, the domain a* of *Catassembler* strand combines with the toehold of domain a in *Substrate* to initiate the first round of TMSDR; after a displacement reaction, the *By-product* strand on *Substrate* is replaced with the *Catassembler* strand, yielding a complex called *Intermediate* having a newly generated toehold of domain c; then the *Fuel* strand binds to the toehold of domain c to initiate a new round of TMSDR, thereby displacing *Catassembler* and *Trigger* while producing a complex called *Waste*; the displaced *Catassembler* is recycled to restart next round of reactions in the catassembly DNA circuit. In the PAEs-based subsystem, *Trigger* released from the catassembly DNA-circuit automatically binds to the toehold of domain e on the *Linker* strand to displace the *Protector* strand from *Duplex-linker′*, thereby exposing self-complementary sticky ends (domain f) to cause self-assembly of PAEs (Fig. 1*A*). In the experiment, we just need to add all of the ingredients to the solution in the PCR tube without further manipulation, and the PAE assemblies will automatically sediment at the bottom of the tube without being disturbed.

Time-Dependent Interaction Scheme for PAE Assembly. We first created a unary system by assigning self-complementary sequences to sticky ends (the f/f domains) on PAEs (Fig. 1*B*), which were reported to assemble into a face-centered cubic (FCC) lattice under thermal annealing (22, 23). As shown in the small angle X-ray scattering (SAXS) data of our experiments, adding a full amount of *Duplex-linker* to the energy-invariant system immediately led to disordered aggregation (Fig. 1*E*, "Before annealing" curve) and an FCC lattice after thermal annealing ("After annealing" curve in Fig. 1*E*) that was in agreement with the theoretical FCC structure (Fig. 1*E*, gray line), replicating the results of an earlier report (22). Regarding the temperature-invariant time-dependent interaction system shown in Fig. 1*A*, fluorescence measurements showed delayed *Trigger* release kinetics when less *Catassembler* was added (*SI Appendix*, Fig. S6*B*), which correspondingly decelerated the assembly of PAEs measured by UV-vis absorption spectroscopy in *SI Appendix*, Fig. S8*B*. In the experiment, a full amount of 1.5-μM *Trigger* (using twice the number of *Duplex-linker′* to

ensure full activation of the protected sticky ends) was directly added to realize the fastest assembly, disordered PAE aggregates emerged (Fig. 1*C*, "Control" curve); by driving the catassembly DNA circuit with 0.5-nM *Catassembler* for the slow release of *Trigger*, an FCC lattice resulted (Fig. 1*C*, "Catassembly" curve). The inability to resolve the third- and fourth-order peaks (Fig. 1*D*, "50 nM" curve) indicates massive disordered components resulting from the rapid release of *Trigger* induced by the addition of more *Catassembler*. With the reduction of *Catassembler* concentration from 50 to 0.5 nM, the representative FCC peaks changed from blurred to sharp (Fig. 1*D*), indicating the improvement of crystalline quality. Generally, this strategy takes longer (~18 h) than the thermal annealing time (~4 h). The strategy was also systematically examined by changing the DNA linker density (*SI Appendix*, Figs. S9 and S10) and size (*SI Appendix*, Fig. S11) of the PAEs. Moreover, the kinetics for the formation of the FCC lattice in the time-dependent interaction system were investigated (*SI Appendix*, Fig. S12).

Given that the slow release of the *Trigger* strands from the catassembly DNA circuits can lead to the ordered structures, we conducted a controlled experiment to simulate this process by manually adding the *Trigger* strands slowly and dropwise. To this end, we first obtained three standard fluorescence curves (slow, medium, and fast release) by adding 2-, 5-, and 50-nM *Catassembler* to the DNA circuit (*SI Appendix*, Fig. S13*A*); we then used a fluorescent *Reporter* for characterization to track the actual amount of the *Trigger* strands released into the solution at different times over a period of 24 h. When 50- and 5-nM *Catassembler* were added, almost all of the *Trigger* strands (1.4 μM of the entire 1.5-μM *Trigger* that hybridized to *Substrate*) were released from the *Substrate* in 1 and 24 h, respectively; when a 2-nM *Catassembler* was added, incomplete release (0.9 μM) occurred within 24 h. Because 0.75-μM *Trigger* strands (the same number with the protected sticky ends on the *dPAE*) are sufficient to induce complete assembly of PAEs, thus PAEs were assembled into FCC lattice in the presence of 2-nM *Catassembler* (Fig. 1*D* and *SI Appendix*, Fig. S8*B*).

We manually added the *Trigger* strands to the PAEs-based subsystems drop by drop over time based on the number of the *Trigger* strands marked in these curves (*SI Appendix*, Fig. S13*A*). As shown in *SI Appendix*, Fig. S13*C*, rapid addition (a total of 1.4-μM *Trigger* strands were added at the beginning) caused disordered PAE aggregates; medium-speed addition (referring to the dots on the blue curve of 5 nM in *SI Appendix*, Fig. S13*A*; 1.4-μM *Trigger* strands were added in 12 times in 24 h) induced the formation of an FCC lattice; slow addition (referring to the dots on the orange curve of 2 nM in *SI Appendix*, Fig. S13*A*; 0.9-μM *Trigger* strands were added in 12 times in 24 h) resulted in a more ordered FCC lattice. More details on manually adding strategy can be found in *SI Appendix*, section S2.6. Based on these experiments, we proved that the ordered structure was indeed caused by the slow addition of the *Trigger* strands.

To assess the generality of the strategy, we then created a binary system by assigning a pair of non-self-complementary sequences to sticky ends (the g/g* domains) on two types of PAEs (*SI Appendix*, Fig. S15), which were reported to form a body-centered cubic (BCC) lattice under thermal annealing (22, 23). In our experiment (e.g., *SI Appendix*, Fig. S16*F*), the assemblies that were disordered at room temperature ("Before annealing" curve) formed a BCC lattice upon thermal annealing ("After annealing" curve) in the energy-invariant system; regarding the time-dependent interaction system, a disordered aggregate was obtained again for fast PAE assembly by adding a full amount of *Trigger* once (the "Control" line), but a BCC lattice formed upon assembling slowly under controlled release of *Trigger* (the "Catassembly" curve).

Mechanism for Realization of Ground State in Time-Dependent Interaction System. To date, thermal annealing for mediating entropy is the commonly adopted way to converge to the ground state. The time-dependent interaction for mediating enthalpy developed here offers an entirely different option that allows "walking" along different paths on the free-energy landscape. We have demonstrated the capability of a time-dependent interaction scheme for the realization of ordered structures in a temperature-invariant system. To understand the underlying mechanism, recall that there are generally two types of dynamic pathways in self-assembly: near-equilibrium pathways that are simply determined by thermodynamic factors and far-from-equilibrium pathways that strongly depend on dynamic effects. Assembling PAEs through DNA hybridization is a typical far-from-equilibrium process because, compared with the structural growth of PAE assemblies, the linkers made of DNA molecules sample their configuration space more slowly (24). Competition between diverse time scales leads to "walking" on the free-energy landscape that is largely dependent on dynamic effects. Thus, directly adding a full amount of *Duplex-linker* (referred to above as an energy-invariant system in Fig. 1*B*) will mostly cause a nonequilibrium process that easily falls into kinetically trapped states to generate a disordered structure (Fig. 1*E*) (25, 26). In the time-dependent interaction system (Fig. 1*A*), the minimum increment ΔE in internal energy depends on the binding energy ΔE of a sticky end, i.e., the f domain having a self-complementary sequence of $^{5'}$-GCGC$^{3'}$ with a binding energy of −7.33 kcal/mol. Driven by the *Trigger* strand continuously released from the catassembly DNA circuit, the system evolves to pass a discrete set of energy levels with an interval ΔE. If the process develops slowly enough, the system may have a long residence time at each energy level to achieve a near-equilibrium state. As the interaction between particles grows, the system experiences a series of near-equilibrium states that eventually converge to the ground state. The small incremental value of internal energy resulting from weak binding of the individual sticky ends facilitates rapid switching between the binding and unbinding of the sticky ends, which is important for exploiting thermal fluctuations to quickly sample the bound configuration so that the system is capable of evading the kinetic "traps" that are generated with incorrectly bound PAEs (27, 28).

Advantages of Time-Dependent Interaction Strategy. In materials science, one of the ultimate goals of nanoscientists is to manipulate the bonds between colloidal particles to produce complex functional materials, much like chemists manipulate chemical bonds to synthesize complex molecules (29). To achieve this goal, consider again that in PAEs, the programmability of these atom equivalents should be optimized so that colloid bonding and colloid assembly can be synchronized, thereby to precisely control their spatiotemporal distribution. However, due to the intrinsic kinetic-trap nature of PAE assembly, the compromise scheme with a two-step operation, first performing hybridization of DNA molecules and then thermal annealing (8, 22), serves as a standard procedure to circumvent this difficulty and obviously does not meet this synchronization requirement. Driven by the catassembly DNA circuits, the strategy that leverages the optimal programmability of PAEs via accounting entirely for the sequence information of all participating DNA molecules is capable of synchronizing the PAE bonding with its assembly. To date, well-developed dynamic DNA nanotechnology allows construction of sophisticated DNA circuits to perform complex tasks (30, 31), and different kinds of PAEs capable of forging new "element tables" using nanoparticle-based building blocks enable the creation of abundant periodic structures, however, these two subfields remain relatively isolated, and there are not many examples of overlap between these disciplines (13, 32). This strategy provides a solution for building an "interface" to bridge the gap between dynamic DNA nanotechnology and PAE

programming, which represents an important step for nanoscientists to manipulate colloidal bonds for creating complex nanomaterials.

From a material manufacturing viewpoint, for the thermal annealing approach, effective assembly occurs in the vicinity of the melting point, while operation is generally carried out at temperatures above the melting point. Entropy still strongly contributes within this temperature span, which will cause significant perturbation of the colloid motion by thermal energy, which is harmful to the assembly. In contrast, the strategy here allows operation at an appointed low temperature such as room temperature on demand that facilitates suppression of this entropy effect.

Conditionally Initiating PAE Assembly by Selectively Activating PAE Bonding. After developing this enthalpy-mediated PAE assembly strategy, we started to explore its versatility to program the bonding of PAEs for complex assemblies. To this end, we created an asymmetric binary system having a pair of non-self-complementary sticky ends (the g/g* domains) (Fig. 2*A*). Two types of PAEs grafted with asymmetric DNA molecular architectures were prepared, as shown in *SI Appendix*, Fig. S18: *PAE-1* bearing a dual DNA duplex complex named *Dual-duplex-linker* and *PAE-2* bearing a single DNA duplex complex named *Duplex-linker*. A BCC structure emerged via thermal annealing treatment (Fig. 2 *A*, *Right*). We changed *Dual-duplex-linker* on *PAE-1* into the architecture shown in *dPAE-1* (Fig. 2 *B*, *Left,* and *SI Appendix*, Fig. S19), covering the sticky end to make it deactivated against *PAE-2*; *dPAE-1* was reactivated by reconfiguring the DNA molecular structure back into the *Dual-duplex-linker* with help of *Trigger* released from catassembly DNA circuit. We observed a BCC lattice upon slow controlled release of *Trigger* by adding less *Catassembler* (Fig. 2*C*). In a similar principle for modifying *PAE-2* into *dPAE-2* (Fig. 2 *B*, *Right,* and *SI Appendix*, Fig. S19), we observed an AlB_2 lattice (Fig. 2*C*).

Why were two different PAE phases obtained in the experiment? In our asymmetric binary system, the hydrodynamic radius ratio of *PAE-2*/*PAE-1* was intentionally designed to be ~0.6. According to previous work by Kim et al. (33), a higher linker ratio (defined as the ratio between the numbers of active linkers per particle) of *PAE-2*/*PAE-1* favored a BCC lattice, while a lower linker ratio of *PAE-2*/*PAE-1* favored an AlB_2 lattice. Consistent with the observation, when *dPAE-1* is gradually activated

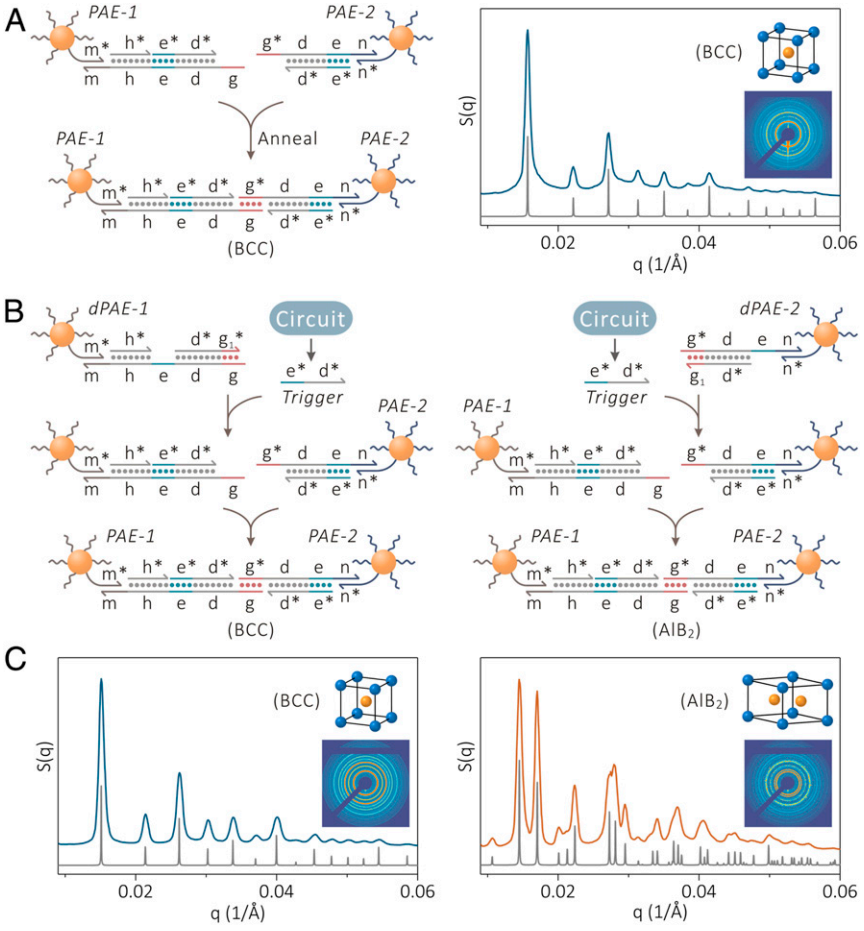

Fig. 2. Programming PAE bonding in an asymmetric binary system using a DNA strand-displacement circuit to conditionally activate PAE assemblies for the realization of different ordered structures. (*A*) Scheme of PAE assembly with a thermal annealing strategy (*Left*), where *PAE-1* has a dual DNA duplex complex with a sticky end of $^{3'}$-TTCCTT$^{5'}$ and *PAE-2* has a single DNA duplex complex with another sticky end of $^{3'}$-AAGGAA$^{5'}$. SAXS patterns of the obtained BCC lattice and the corresponding unit cell model (*Right*). [*PAE-1*] = 6 nM, [*PAE-2*] = 24 nM, [*Dual-duplex-linker*] = 480 nM, and [*Duplex-linker*] = 960 nM. (*B*) Scheme of programming PAE bonding for the realization of conditional activation of PAE assemblies (see *SI Appendix*, Fig. S19 for details). (*C*) SAXS data of the BCC lattice when *PAE-1* was modified into *dPAE-1* (*Left*) and the AlB_2 lattice when *PAE-2* was modified into *dPAE-2* (*Right*), both of which were driven by slow release of *Trigger* from the catassembly DNA circuit. The gray curves represent the theoretical SAXS patterns for perfect BCC and AlB_2 lattices. Here, for the BCC structure [*dPAE-1*] = 6 nM, [*PAE-2*] = 24 nM, [*Dual-duplex-linker′*] = 480 nM, [*Duplex-linker*] = 960 nM, [*Substrate*] = 960 nM, [*Fuel*] = 1.92 μM, and [*Catassembler*] = 2 nM; for the AlB_2 structure [*PAE-1*] = 6 nM, [*dPAE-2*] = 24 nM, [*Dual-duplex-linker*] = 480 nM, [*Duplex-linker′*] = 960 nM, [*Substrate*] = 1.92 μM, [*Fuel*] = 3.84 μM, and [*Catassembler*] = 2 nM.

into *PAE-1*, *PAE-2*/*PAE-1* maintains a relatively high linker ratio, BCC lattice is formed (Fig. 2 *B*, *Left*). In contrast, when *dPAE-2* is activated, *PAE-2*/*PAE-1* maintains a low linker ratio, the AlB_2 lattice is formed (Fig. 2 *B*, *Right*). It is reasonable to suppose that our asymmetric binary system should be near the boundary of the BCC and AlB_2 phases, thus the two resulted PAE aggregates are located in different regions of the PAE phase diagram drawn by Macfarlane et al. (10). Compared with thermal annealing, which yielded only one ordered structure (BCC lattice), the time-dependent interaction scheme enabled the production of two ordered structures (BCC and AlB_2 lattices) through slight modification of *PAE-1* or *PAE-2* without altering the topology of the catassembly DNA circuit and base sequences of DNA molecules, revealing the capabilities of this strategy for programming the bonding of PAEs to control their assembly and exemplifying the power of the current approach to conditionally and dynamically activate PAE bonding by selectively manipulating PAEs functionalized with distinct asymmetric architecture of DNA molecules.

PAE Lattice Transition through Dynamically Switching Bonding Identity. The implementation of adaptable and switchable structures for dynamically controlling material properties is an exciting but challenging task. In general, an intractable procedure for dynamically changing the shape of particles or interaction between particles was required to realize this structural transformation (12, 34). Zhang et al. developed a way to control PAE lattice switching by postmodification of DNA shells to selectively regulate the attractive or repulsive potential between PAE particles (13). Kim et al. obtained a switchable structure by creating "transmutable nanoparticles" having reconfigurable DNA molecules that allowed the nanoparticles to be conditionally activated or deactivated in response to external stimuli (33). Considering that the bonding identity of a PAE is dictated by its sticky ends, we attempted to demonstrate the capability of this time-dependent interaction scheme for manipulating PAEs by dynamically changing the base sequence of the sticky ends, thereby implementing the transformation of the PAE lattices.

For this purpose, a liquid solution containing BCC solid crystals was prepared a priori by thermal annealing in a binary system having a pair of non-self-complementary sticky ends (the g/g* domains) as illustrated in *SI Appendix*, Fig. S21. Within this solution, once *Trigger* carrying a self-complementary sticky end (domain f) was released from the catassembly DNA circuit, it displaced both non-self-complementary sticky ends on the two types of PAEs (*PAE-1* and *PAE-2*) and led to all PAEs carrying the self-complementary sticky end with an identical sequence (*PAE*); accordingly, the binary system was switched into a unary system (Fig. 3*A* and *SI Appendix*, Fig. S22). Correspondingly, the structure was expected to transform from a BCC lattice to an FCC lattice. Here, we intentionally designed a higher melting temperature (T_m) for the unary system ($T_{m2} \sim 57$ °C) and a lower one for the binary system ($T_{m1} \sim 34$ °C) (*SI Appendix*, Fig. S24). At a temperature between the melting points of the two systems (40 °C), the BCC crystals were first melted into dispersed PAEs (fluid), and then FCC crystals formed by slowly releasing *Trigger* (Fig. 3*B* and *SI Appendix*, Fig. S25). *Trigger* released from the catassembly DNA circuit served two purposes: deactivating the existing sticky end and creating a new sticky end so that the sticky end can be dynamically switched. For this structural transformation process, the kinetics-dependent manner occurred as expected, and the rapid release of *Trigger* led to a disordered aggregate (*SI Appendix*, Fig. S25, "50 nM" curve), while the slow release of *Trigger* produced an ordered FCC structure (*SI Appendix*, Fig. S25, "0.5 nM" curve).

Conversely, at a temperature lower than the melting point of the binary system (25 or 30 °C), direct transformation from the BCC phase to the FCC phase occurred in a solid-solid transition way (*SI Appendix*, Figs. S23 and S26). *SI Appendix*, Fig. S26 indicated that it is not necessary to release *Trigger* slowly. Using a 10- to 50-nM *Catassembler* to release *Trigger* faster can achieve a perfect solid–solid phase transition. Through observing the time evolution of the solid–solid transition via simulating the fastest release of *Trigger* by adding all 1.5-μM *Trigger* strands at once, we found that the process experienced a disorder-like period before transforming into the FCC lattice structure (*SI Appendix*, Fig. S27); that is, the process started with the BCC lattice, then underwent disorderly aggregation, and finally reached the FCC lattice. It is conceivable that adding enough *Trigger* strands can quickly break the bonds in the BCC lattice, thus forcing the system to jump from the low free-energy state of the BCC lattice to the high free-energy state of the disordered structure, from which the system may automatically evolve to low free-energy state of FCC structure in the presence of *Trigger* strands with self-complementary sticky ends. Thus, Fig. 3*B* and *SI Appendix*, Fig. S26 illustrate how an identical ordered structure is realized by experimenting at two different temperatures.

With the same principle, a unary system having a self-complementary sticky end with a thermal-annealed FCC lattice as a nascent structure (*SI Appendix*, Fig. S28), releasing two *Trigger* strands having a pair of non-self-complementary sticky ends from two distinct DNA circuits to displace the self-complementary sticky ends on PAEs caused the system to switch from a unary system to a binary system (Fig. 3*C* and *SI Appendix*, Fig. S29); correspondingly, the structure was expected to transform from an FCC lattice into a BCC lattice. When the unary system and binary system were rationally designed to have different melting temperatures ($T_{m1} \sim 37$ °C and $T_{m2} \sim 51$ °C, respectively) (*SI Appendix*, Fig. S30), the transformation from the FCC lattice to the BCC lattice was observed at 40 °C (Fig. 3*D* and *SI Appendix*, Fig. S31).

This enthalpy-mediated PAE lattice transformation strategy (Fig. 3) offers an example of dynamically switching the PAE identities, which is realized by replacing the original sticky end with a new one as assembly is progressing. In fact, the identities of PAEs can be switched not only by altering the sticky ends but also by completely changing the outer-layer DNA molecules. Furthermore, considering the catassembly DNA circuit, the sequence of the input *Catassembler* strand, which may be present a priori in the environment or be released from another DNA circuit, is independent of that of the output *Trigger* strand. This orthogonality allows arbitrary sequence design of input DNA molecules for DNA sequence exchange by outputting different sequences of *Trigger* strands, thereby to construct complex reaction systems by cascading different DNA circuits.

Programming PAE Bonding for the Formation of Binary AuNP-Protein Lattice. The programmable coassembly of multiple nanoscale building blocks with disparate chemical and physical properties, including different inorganic nanoparticles (e.g., Fe_3O_4, Pt, and quantum dots) (5, 13) and biomolecules (e.g., proteins) (35–37) is of great potential in the applications of catalysis, sensing, and photonics. However, for thermal annealing, the strict melting temperature limits the participation of biomolecules, because the intrinsic temperature-sensitive biomolecule such as protein may suffer from possible denaturation upon annealing treatment at a high temperature. This drawback limits the complexity and functionality of programming PAE bonding. The low operation temperature of our proposed enthalpy-mediated scheme using the time-dependent interaction surely facilitates the treatment of such a temperature-sensitive biomolecule. To this end, we constructed a binary AuNP-protein assembly system programmed by the enthalpy-mediated strategy (Fig. 4*A* and *SI Appendix*, Fig. S32), where *dPAE-1* with a AuNP core possesses protected sticky ends and *PAE-2* with a core of tetrameric heme-containing enzyme possesses active sticky ends. A CsCl lattice was formed at room temperature under programming of the catassembly DNA circuit in the presence of 5-nM *Catassembler* as demonstrated by the simple cubic scattering patterns shown in Fig. 4*B* (the scattering of the

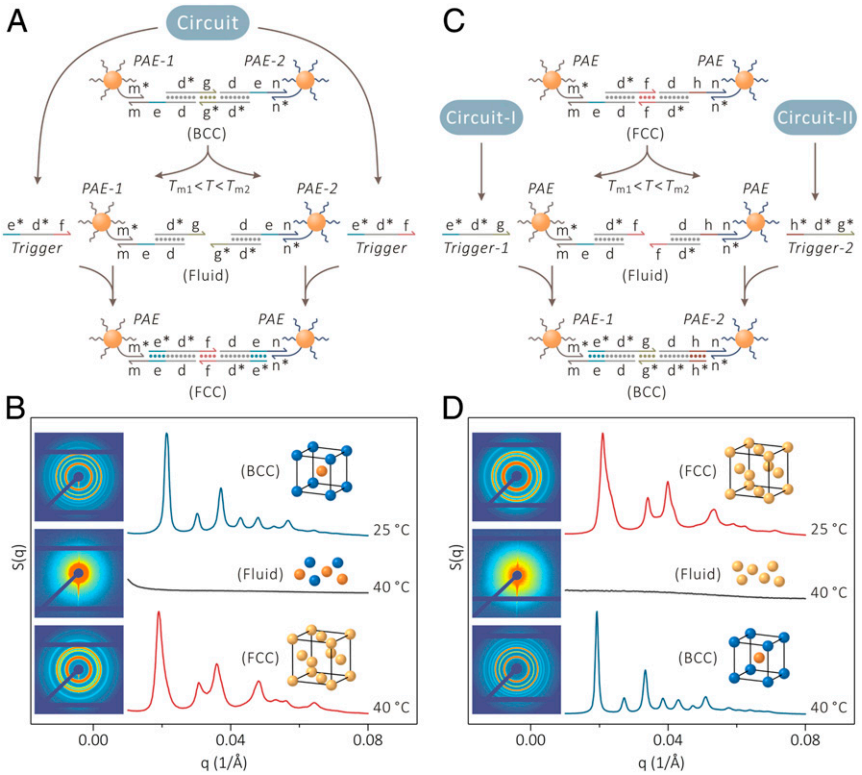

Fig. 3. Programming PAE bonding using DNA strand-displacement circuits to dynamically change PAE identities for dynamic transformations of PAE lattices. (*A*) Scheme for dynamically switching a binary system ($T_{m1} \sim 34$ °C) having non-self-complementary sticky ends of $^{5'}$-AAGGAA$^{3'}$ and $^{5'}$-TTCCTT$^{3'}$ on *PAE-1* and *PAE-2*, respectively, into a unary system ($T_{m2} \sim 57$ °C) having a self-complementary sticky end of $^{5'}$-TGCGCA$^{3'}$ on all PAEs. A detailed mechanism can be found in *SI Appendix*, Fig. S22. (*B*) SAXS patterns for transforming from a BCC lattice (*Top*) to an FCC lattice (*Bottom*) at 40 °C in a solid–fluid–solid transition. Here, [*PAE-1*] = [*PAE-2*] = 12.5 nM, [*Duplex-linker-1*] = [*Duplex-linker-2*] = 500 nM, [*Substrate*] = 1.5 μM, [*Fuel*] = 3 μM, and [*Catassembler*] = 0.5 nM. (*C*) Scheme for dynamically switching a unary system ($T_{m1} \sim 37$ °C) having a self-complementary sticky end of $^{5'}$-TAGCTA$^{3'}$ on all PAEs into a binary system ($T_{m2} \sim 51$ °C) having non-self-complementary sticky ends of $^{5'}$-GGAAGG$^{3'}$ and $^{5'}$-CCTTCC$^{3'}$ on *PAE-1* and *PAE-2*, respectively. A detailed mechanism can be found in *SI Appendix*, Fig. S29. (*D*) SAXS data for PAEs transformed from an FCC lattice (*Top*) to a BCC lattice (*Bottom*) at 40 °C in a solid–fluid–solid transition. Here, [*PAE*] = 25 nM, [*Duplex-linker-1*] = [*Duplex-linker-2*] = 500 nM, [*Substrate-1*] = [*Substrate-2*] = 750 nM, [*Fuel*] = 3 μM, and [*Catassembler*] = 0.5 nM.

proteins was negligible compared with that of the AuNPs in the practical SAXS measurements).

Conclusion

The enthalpy-mediated strategy provides a general solution for programming PAE bonds. Combining the complex functions of DNA strand-displacement circuits (30, 31) with sophisticated DNA functional building blocks such as "transmutable nanoparticles" (33), DNA-origami-based units (38, 39), and the methods for regulating the attractive and repulsive forces between particles (13) can greatly increase the possibilities for the creation of complex and functional nanoscale materials and for the realization of complex phase behaviors (12, 34). Moreover, this time-dependent interaction scheme may offer additional possibilities for creating artificial matter that possesses properties of living matter (14, 15) to aid in new discoveries.

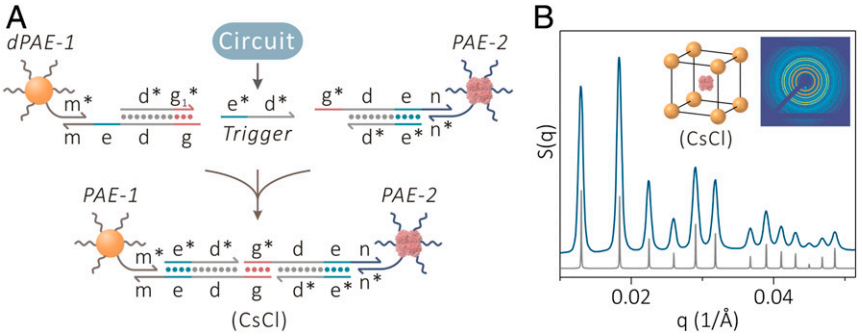

Fig. 4. Formation of a binary AuNP-protein superlattice at room temperature. (*A*) Scheme for the assembly of *dPAE-1* and *PAE-2* programmed by the DNA strand-displacement circuit in a binary system, where *dPAE-1* denotes the DNA-AuNP conjugate and *PAE-2* denotes the DNA-protein conjugate. (*B*) The obtained SAXS patterns of the simple cubic lattice indicated the formation of a CsCl crystal structure (the corresponding unit cell model is shown in the *Inset*) in the binary AuNP-protein assembly system. The gray curve represents the theoretical SAXS pattern for a simple cubic lattice. Here, [*dPAE-1*] = [*PAE-2*] = 25 nM, [*Duplex-linker-1′*] = [*Duplex-linker-2*] = 1 μM, [*Substrate*] = 2 μM, [*Fuel*] = 4 μM, and [*Catassembler*] = 5 nM.

Materials and Methods

Materials. The 10-nm AuNPs were obtained from nanoComposix. *Corynebacterium glutamicum* (*Cg*) catalase was purchased from Sigma-Aldrich. All DNA sequences used in this work (*SI Appendix*, Tables S1–S6) were synthesized by Sangon Biotechnology Co., Ltd. More details regarding the materials can be found in *SI Appendix*, section S1.1.

Preparation of DNA Substrate. The detailed experimental procedures for preparation and purification of DNA substrate used in DNA circuit can be found in *SI Appendix*, section S1.2.

Preparation of PAEs. DNA linkers with different architectures were prepared at first (*SI Appendix*, section S1.3). Then, DNA-AuNPs were prepared by grafting thiolated oligonucleotides on surface of AuNPs through a "salt aging" process (more detailed information can be found in *SI Appendix*, section S1.4). The quantification method of the number of thiolated DNA strands on each AuNP can be found in *SI Appendix*, section S1.5. DNA-proteins were obtained according to the method described in *SI Appendix*, section S1.6. Last, PAEs were prepared through hybridization of DNA linkers and DNA-AuNPs or DNA-proteins; detailed process can be found in *SI Appendix*, section S1.7.

Kinetic Characterization. The setup process for PAE assembly system driven by DNA circuit can be found in *SI Appendix*, section S1.8. The performance of the DNA circuit was investigated via real-time fluorescence kinetic measurements (see *SI Appendix*, section S2.1 for details). The aggregation kinetics of the PAE assembly driven by the DNA circuit was studied using a UV-vis spectrophotometer (see *SI Appendix*, section S2.2 for details).

Thermal Annealing. Detailed methods for test of melting temperatures of PAE aggregates and preparation of PAE assemblies through thermal annealing were described in *SI Appendix*, section S1.9.

SAXS Characterization. All SAXS experiments for characterization of PAE assemblies were performed at the BL16B1 beamline of the Shanghai Synchrotron Radiation facility. For more details, see *SI Appendix*, section S1.10.

Data Availability. All data discussed in the paper are included in the main text and *SI Appendix*.

ACKNOWLEDGMENTS. We gratefully acknowledge BL16B1 beamline of the Shanghai Synchrotron Radiation Facility for supporting the SAXS tests. We thank Prof. Wei Jiang (Changchun Institute of Applied Chemistry) for insightful discussion. This work was supported by the National Natural Science Foundation of China (Grants 21991132, 21434007, and 91427304), the Fundamental Research Funds for the Central Universities (Grants WK3450000002 and WK2060200026), the Financial Grant from the China Postdoctoral Science Foundation (2018M630708), the National Postdoctoral Program for Innovative Talents (BX20180285), the Research Fund of Hefei National Laboratory for Physical Sciences at the Microscale Grant (SK2340000001), and the Open Research Fund of State Key Laboratory of Polymer Physics and Chemistry (Changchun Institute of Applied Chemistry, Chinese Academy of Sciences).

1. W. Ostwald, Studies on the formation and transformation of solid bodies. *Z. Phys. Chem.* **22**, 289–330 (1897).
2. P. Rein ten Wolde, D. Frenkel, Homogeneous nucleation and the Ostwald step rule. *Phys. Chem. Chem. Phys.* **1**, 2191–2196 (1999).
3. C. Desgranges, J. Delhommelle, Controlling polymorphism during the crystallization of an atomic fluid. *Phys. Rev. Lett.* **98**, 235502 (2007).
4. K. A. Dill, S. Bromberg, *Molecular Driving Forces: Statistical Thermodynamics in Biology, Chemistry, Physics, and Nanoscience* (Garland Science, New York, ed 2, 2010).
5. C. Zhang *et al*., A general approach to DNA-programmable atom equivalents. *Nat. Mater.* **12**, 741–746 (2013).
6. R. J. Macfarlane, M. N. O'Brien, S. H. Petrosko, C. A. Mirkin, Nucleic acid-modified nanostructures as programmable atom equivalents: Forging a new "table of elements". *Angew. Chem. Int. Ed. Engl.* **52**, 5688–5698 (2013).
7. R. J. Macfarlane *et al*., Importance of the DNA "bond" in programmable nanoparticle crystallization. *Proc. Natl. Acad. Sci. U.S.A.* **111**, 14995–15000 (2014).
8. D. Nykypanchuk, M. M. Maye, D. van der Lelie, O. Gang, DNA-guided crystallization of colloidal nanoparticles. *Nature* **451**, 549–552 (2008).
9. W. Cheng *et al*., Free-standing nanoparticle superlattice sheets controlled by DNA. *Nat. Mater.* **8**, 519–525 (2009).
10. R. J. Macfarlane *et al*., Nanoparticle superlattice engineering with DNA. *Science* **334**, 204–208 (2011).
11. C. R. Laramy *et al*., Controlled symmetry breaking in colloidal crystal engineering with DNA. *ACS Nano* **13**, 1412–1420 (2019).
12. W. B. Rogers, V. N. Manoharan, Programming colloidal phase transitions with DNA strand displacement. *Science* **347**, 639–642 (2015).
13. Y. Zhang *et al*., Selective transformations between nanoparticle superlattices via the reprogramming of DNA-mediated interactions. *Nat. Mater.* **14**, 840–847 (2015).
14. Z. Zeravcic, M. P. Brenner, Spontaneous emergence of catalytic cycles with colloidal spheres. *Proc. Natl. Acad. Sci. U.S.A.* **114**, 4342–4347 (2017).
15. Z. Zeravcic, V. N. Manoharan, M. P. Brenner, Colloquium: Toward living matter with colloidal particles. *Rev. Mod. Phys.* **89**, 031001 (2017).
16. B. Yurke, A. J. Turberfield, A. P. Mills, F. C. Simmel, J. L. Neumann, A DNA-fuelled molecular machine made of DNA. *Nature* **406**, 605–608 (2000).
17. T. Song, H. Liang, Synchronized assembly of gold nanoparticles driven by a dynamic DNA-fueled molecular machine. *J. Am. Chem. Soc.* **134**, 10803–10806 (2012).
18. D. Yao *et al*., Integrating DNA-strand-displacement circuitry with self-assembly of spherical nucleic acids. *J. Am. Chem. Soc.* **137**, 14107–14113 (2015).
19. W. B. Rogers, W. M. Shih, V. N. Manoharan, Using DNA to program the self-assembly of colloidal nanoparticles and microparticles. *Nat. Rev. Mater.* **1**, 16008 (2016).
20. D. Y. Zhang, A. J. Turberfield, B. Yurke, E. Winfree, Engineering entropy-driven reactions and networks catalyzed by DNA. *Science* **318**, 1121–1125 (2007).
21. Y. Wang *et al*., What molecular assembly can learn from catalytic chemistry. *Chem. Soc. Rev.* **43**, 399–411 (2014).
22. S. Y. Park *et al*., DNA-programmable nanoparticle crystallization. *Nature* **451**, 553–556 (2008).
23. R. J. Macfarlane *et al*., Assembly and organization processes in DNA-directed colloidal crystallization. *Proc. Natl. Acad. Sci. U.S.A.* **106**, 10493–10498 (2009).
24. S. Whitelam, R. L. Jack, The statistical mechanics of dynamic pathways to self-assembly. *Annu. Rev. Phys. Chem.* **66**, 143–163 (2015).
25. S. Vial, D. Nykypanchuk, K. G. Yager, A. V. Tkachenko, O. Gang, Linear mesostructures in DNA–nanorod self-assembly. *ACS Nano* **7**, 5437–5445 (2013).
26. S. Whitelam *et al*., The impact of conformational fluctuations on self-assembly: Cooperative aggregation of archaeal chaperonin proteins. *Nano Lett.* **9**, 292–297 (2009).
27. D. C. Rapaport, Role of reversibility in viral capsid growth: A paradigm for self-assembly. *Phys. Rev. Lett.* **101**, 186101 (2008).
28. J. Grant, R. L. Jack, S. Whitelam, Analyzing mechanisms and microscopic reversibility of self-assembly. *J. Chem. Phys.* **135**, 214505 (2011).
29. M. R. Jones, N. C. Seeman, C. A. Mirkin, Programmable materials and the nature of the DNA bond. *Science* **347**, 1260901 (2015).
30. L. Qian, E. Winfree, Scaling up digital circuit computation with DNA strand displacement cascades. *Science* **332**, 1196–1201 (2011).
31. K. M. Cherry, L. Qian, Scaling up molecular pattern recognition with DNA-based winner-take-all neural networks. *Nature* **559**, 370–376 (2018).
32. Y. Kim, R. J. Macfarlane, C. A. Mirkin, Dynamically interchangeable nanoparticle superlattices through the use of nucleic acid-based allosteric effectors. *J. Am. Chem. Soc.* **135**, 10342–10345 (2013).
33. Y. Kim, R. J. Macfarlane, M. R. Jones, C. A. Mirkin, Transmutable nanoparticles with reconfigurable surface ligands. *Science* **351**, 579–582 (2016).
34. Y. Zhang, F. Lu, D. van der Lelie, O. Gang, Continuous phase transformation in nanocube assemblies. *Phys. Rev. Lett.* **107**, 135701 (2011).
35. J. D. Brodin, E. Auyeung, C. A. Mirkin, DNA-mediated engineering of multicomponent enzyme crystals. *Proc. Natl. Acad. Sci. U.S.A.* **112**, 4564–4569 (2015).
36. K. Krishnamoorthy *et al*., Defining the structure of a protein–spherical nucleic acid conjugate and its counterionic cloud. *ACS Cent. Sci.* **4**, 378–386 (2018).
37. J. R. McMillan, O. G. Hayes, P. H. Winegar, C. A. Mirkin, Protein materials engineering with DNA. *Acc. Chem. Res.* **52**, 1939–1948 (2019).
38. W. Liu *et al*., Diamond family of nanoparticle superlattices. *Science* **351**, 582–586 (2016).
39. S. Woo, P. W. K. Rothemund, Programmable molecular recognition based on the geometry of DNA nanostructures. *Nat. Chem.* **3**, 620–627 (2011).